2005-01-2935

# Modeling of a Loop Heat Pipe for Ground and Space Conditions

**Valeri V. Vlassov and Roger R. Riehl**
National Institute for Space Research – INPE/DMC-Satelite



## ABSTRACT

This paper presents a mathematical model of a LHP, where its results were compared with experimental test results and the LHP behavior was predicted for Space conditions. In the LHP condenser, the condensate film thickness in the tube is determined by the solution of the conjugate equations of energy, momentum and mass balance in the control volume. Evaporator and compensation chamber are both described by a few transient nodes with generalized key parameters, whose values were adjusted by test results. Experimental LHP consists of cylindrical stainless steel evaporator with an integral compensation chamber, where the primary wick is of micropore UHMW polyethylene and the condenser is an aluminum plate, with acetone as the working fluid. The tests conditions have been reproduced in the mathematical model and its parameters were adjusted using the measured temperatures. The model was applied to predict the LHP behavior for Space conditions, corresponding to the circular low Earth equatorial orbit.

## INTRODUCTION

Capillary pumped loops (CPLs) and loop heat pipes (LHPs) are emerging as the baseline design of thermal control systems for space applications because of their efficiency. CPLs were invented in the USA (NASA) in late 60's [1] whereas LHPs appeared in Russia in early 70's [2,3]. Critical reviews were carried out with CPL and LHP showing their similarities and differences have been stated [4,5]. LHP and CPL are the key apparatuses of thermal control in GLAS, EOS-Chemistry, GOES, SWIFT spacecraft and several communications satellites.

While the CPL and LHP technologies have reached a certain level of maturity, many issues still remain as the subjects of active researches. The reason lies in the complex behavior of the two-phase fluid inside the devices. It yields several operation modes and possible types of failure, like eventual evaporator dry-out, degradation of characteristics, pressure oscillations, etc. These modes and failures actually are studied experimentally. The start-up issues of CPLs have been particularly investigated [6,7] among others as well as pressure oscillations were investigated [8-10]. Maidanik [11] reveals the low power limit on start-up and recuperation mode in CPLs. There were several flight missions carrying CPL as scientific payloads and devoted to investigations of its performance under micro-gravity conditions [12-14].

Theoretical studies on CPLs and LHPs at the present are lagged behind the experimental investigations. Most of mathematical models were developed for processes in microscopic level (either for the evaporator or condenser tube) with well-defined fixed boundary conditions. From the broad variety of such models, it can be cited those developed for element of CPL evaporator [15], the evaporation process from meniscus of porous wicks [16], completed researches on evaporation from evaporator bulk of a CPL [17] and the most complete steady-state model of CPL/LHP condenser tube developed by Begg and Khrustalev [18].

At system level quite few models have been developed. An elaborated node-model for a CPL space experiment considering the operation under presence of vapor phase in the liquid channel of the evaporator has been presented in [19]. Cullimore and Baumann [20] developed a most advanced node-type model of LHP, which was directly incorporated into the SINDA/Fluint fluid-thermal analyzer software. Vlassov et. al [21] developed a conception of the CPL/LHP modeling at two levels of detailing, allowing the detailed model to be incorporated in the thermal model of the entire satellite by the most effective way.

Upon analyzing the available models for LHPs, it became necessary to perform a more refined investigation towards the conception and implementation of a mathematical model that could better describe LHPs behavior. Focusing on this matter, this paper explore the LHP modeling conception when the condenser-radiator assembling is simulated by relatively precise sub-model, whereas evaporator/compensation chamber (CC) set is described by a coarse functional sub-model. This sub-model contains several generalized coefficients whose values are adjusted by ground test results obtained in laboratory conditions. Then, the model was used to

predict the LHP behavior in Space conditions, corresponding to a circular low Earth orbit of EQUARS satellite, which is actually under development at INPE.

## LOOP HEAT PIPE MODEL

Modeling the LHP is based on a regular cylindrical capillary evaporator/CC with a single condenser, connected by vapor and liquid lines.

For the proposed model, the capillary evaporator/CC schematically assembly is shown in Fig. 1. Temperature definitions and main nodes of the model are also shown, as well as numerical nodal layout of the radiator plate.

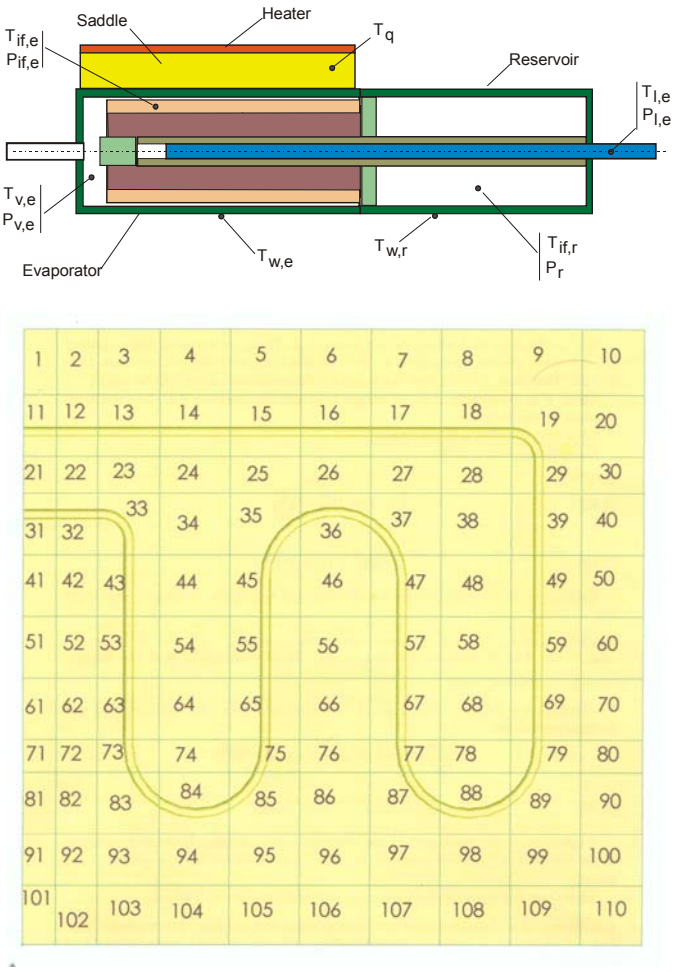


Figure 1. Diagram of nodal layout of the evaporator-reservoir and condenser.

The mass balance in a LHP is based on each-time-step calculation of the amount of fluid present in the tube lines, condenser and evaporator. Therefore, having in hand the liquid inventory used to charge the LHP, the current amount of fluid in the CC is calculated by the loop balance as

$$M_{fres} = M_{charge} - M_{evap} - M_{cond} - M_{vline} - M_{lline}. \quad (1)$$

The two-phase mixture in the CC is suggested to be in the saturation conditions. The vapor density is available from the table of thermophysical properties [23]. The current volumes and masses are defined through the basic equations as follows:

$$V_{vres} = \frac{\rho' V_{res} - M_{fres}}{\rho' - \rho''}, \quad (2)$$

$$V_{lres} = \frac{M_{fres} - \rho'' V_{res}}{\rho' - \rho''}, \quad (3)$$

$$M_{vres} = \frac{\rho''(\rho' V_{res} - M_{fres})}{\rho' - \rho''}, \quad (4)$$

$$M_{lres} = \frac{\rho'(M_{fres} - \rho'' V_{res})}{\rho' - \rho''}. \quad (5)$$

The energy balance of the CC at the interface can be expressed as follows:

$$\left(C'_p V'_{res}\rho' + \frac{1}{2}Cm_{wr}\right)\frac{dT_{\delta r}}{dt} = \lambda\dot{m}_{rc} + G_{\delta r}(T_{wr} - T_{\delta r}) - (1-\varsigma_e)C'_p\dot{m}(T_{\delta r} - T_{le}) + G_{\delta\delta}(T_{\delta e} - T_{\delta r}). \quad (6)$$

It should be noted that the first term is responsible for the thermal effects of eventual evaporation-condensation at the vapor-liquid interface in the CC.

Change of mass of liquid phase in the CC is defined by the difference of fluid mass flow rate incoming from bayonet and liquid mass flow rate passing through the evaporator primary wick for evaporating. Thus, the following expression can be used to represent this parameter and it is derived as:

$$\frac{dM_{lres}}{dt} = (1-x)(\dot{m} + \dot{m}_\delta) - \dot{m}. \quad (7)$$

The basic system of equations, representing the energy balance for the evaporator is presented as:

$$Cm_q\frac{dT_q}{dt} = Q_q(t) - G_{qw}(T_q - T_{we}), \quad (8)$$

$$Cm_{we}\frac{dT_{we}}{dt} = G_{qw}(T_q - T_{we}) - G_{we}(T_{we} - T_{\delta e}) - G_{wr}(T_{we} - T_{wr}), \quad (9)$$

$$Cm_e\frac{dT_{\delta e}}{dt} = G_{we}(T_{we} - T_{\delta e}) - \lambda\dot{m} - \varsigma_e C'_p\dot{m}(T_{\delta e} - T_{le}) - G_{\delta\delta}(T_{\delta e} - T_{\delta r}), \quad (10)$$

$$Cm_{wr}\frac{dT_{wr}}{dt} = G_{wr}(T_{we}-T_{wr}) - G_{\delta r}(T_{wr}-T_{\delta r}) + Q_r(t) - G_{ra}(T_{wr}^4 - T_{ra}^4(t)) - G_{hr}(T_{wr}-T_{ra}(t)), \quad (11)$$

$$C'_p V_{lr}\rho'\frac{dT_{\delta r}}{dt} = G_{\delta r}(T_{wr}-T_{\delta r}) - (1-\varsigma_e)C'_p\dot{m}(T_{\delta r}-T_{le}) + G_{\delta\delta}(T_{\delta e}-T_{\delta r}). \quad (12)$$

The energy balance is written for the saddle (temperature $T_q$), evaporator wall ($T_{we}$), zone of vapor-liquid interface in the evaporator ($T_{\delta e}$), CC wall ($T_{wr}$) and zone of vapor-liquid interface in CC ($T_{\delta r}$).

The main generalized parameters that should be adjusted by tests are the following conductances: $G_{we}$ (between evaporator wall and vapor-liquid interface in the evaporator), $G_{wr}$ (between evaporator wall and CC wall), $G_{\delta r}$ (between CC wall and vapor-liquid interface in the evaporator), $G_{\delta\delta}$ (between vapor-liquid interfaces in the evaporator and CC, through the path: secondary wick – primary wick). One more important parameter is $\zeta$, which defines the fraction of the enthalpy of the incoming cold fluid directed to the evaporator core. The remainder fraction (1-$\zeta$) is directed related to the CC.

The radiator plate model is based on the discretization of the following energy balance equation:

$$C\rho\delta_w\frac{\partial T_w}{\partial t} = \delta_w k_w\frac{\partial^2 T_w}{\partial x^2} + \delta_w k_w\frac{\partial^2 T_w}{\partial y^2} + q_w(t,x,y) - h(T_w - T_a(t)) - \varepsilon\sigma T_w^4, \quad (13)$$

where $T_w \equiv T_w(t,x,y)$ is the radiator plate (wall) temperature and the incoming flux $q_w(t,x,y)$ is defined from the condenser sub-model. The coordinates system is orthogonal one with axes $(x,y)$ laying in the radiator plane and adopted to the rectangular configuration.

The axial momentum conservation for viscous flow in a liquid film is done in the suggestion of the annular flow and that the gravity does not disturb the condensing film. Thus

$$\frac{dP'}{dz} + \rho' g\Delta\bar{y}_g = \mu'\left(\frac{\partial^2 u'}{\partial r^2} + \frac{1}{r}\frac{\partial u'}{\partial r}\right), \quad (14)$$

for the following boundary conditions:

$$u'(R) = 0, \quad (15)$$

$$\left.\frac{\partial u'}{\partial r}\right|_{r=R-\delta} = -\frac{1}{\mu'}\tau'_\delta. \quad (16)$$

The liquid axial mass flow rate along the condenser tube length (curvilinear coordinate z) is obtained by integration over the condenser tube cross-section, which results the expression:

$$\dot{m}' = 2\pi\rho'\int_{R-\delta}^{R} ru(r)dr = -\frac{\pi\rho'\delta^2(2R-\delta)^2}{8\mu}\frac{\partial P'}{\partial z}. \quad (17)$$

From the vapor phase, the tangential stress at vapor-liquid interface is defined as

$$\tau''_\delta = \xi\frac{\rho''(\bar{u}''-u'_\delta)^2}{8}. \quad (18)$$

For the Eq. (18), the condition of equality of stresses at the interface is used.

At each node in the condensation plate, the local energy balance is represented as:

$$\lambda_i\dot{m}_{ci} = G_{\lambda wi}(T_{\delta i}-T_{wi}) - G_{\lambda li}(\bar{T}'_{i-1}-T_{wi}). \quad (19)$$

The left part of (19) provides the incoming flux $q_w(t,x,y)$ value to the radiator plate equation (13).

A special numerical procedure was developed to tackle all equations together yielding reliable convergence. The mathematical model presented here was solved in order to be correlated to experimental data used to validate the model. An experimental test program for LHPs has been developed and the results have been used to adjust the mathematical model.

## EXPERIMENTAL LOOP HEAT PIPE PROGRAM

The experimental LHP (named here as TCD-LHP2) program has been developed on a long-term program to qualify this device for future space applications in Brazil, to manage up to 100 W of applied heat. This program has been used to design, build and test LHPs using alternative working fluids in order to substitute the so-used ammonia as this fluid represents potential hazard as well as expensive purification/charging technology. Thus, the entire program has been focused on the use of acetone in a stainless steel LHP that uses UHMW polyethylene as primary wick. This material selection has been made due to the good compatibility between all internal parts with high grade acetone along time.

The TCD-LHP2 has been tested under laboratory conditions, performing the thermal control on a power cycle mode where low and high heat loads are administrated to the capillary evaporator. The operational conditions are monitored and analyzed over the time in order to properly establish the non-condensable gases (NCGs) influence on the overall LHP performance [22]. The TCD-LHP2 is shown in Fig. 2 and Fig. 3 displays the representation of the set capillary evaporator/CC used to define the mathematical model and validate it.

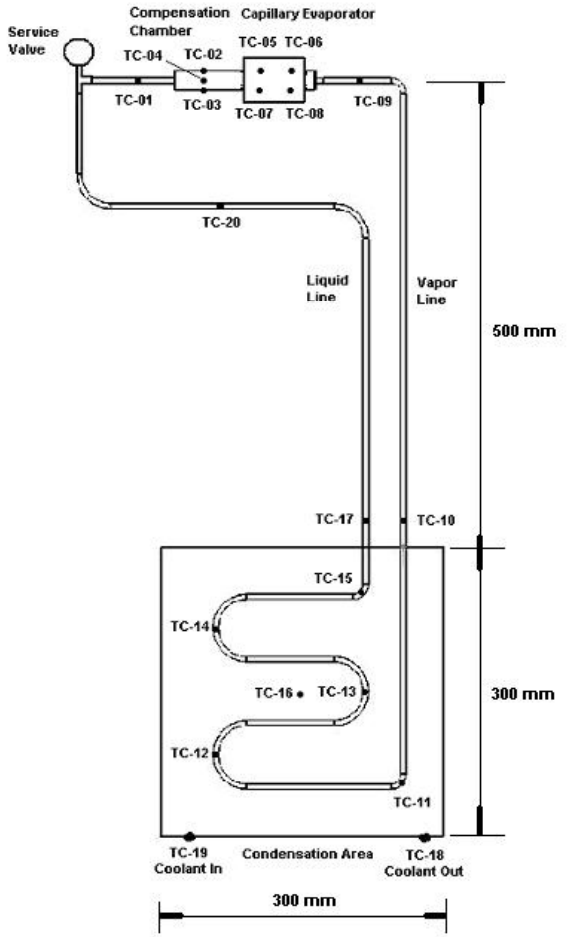


Figure 2. TCD-LHP2 experimental test bed.

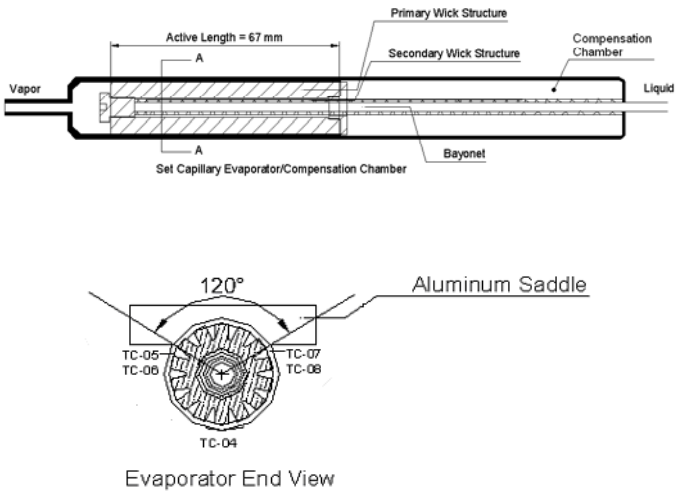


Figure 3. Capillary evaporator/CC configuration on the TCD-LHP2.

The entire LHP was instrumented with 20 type-T thermocouples (deviation of ± 0.3°C at 100 °C) connected to a Agilent 32920A data acquisition system used to monitor the temperatures and save them on a spreadsheet file for further analysis. The condensation plate (300 x 300 mm x 4 mm thick) was composed of a heat exchanger with embedded channels, circulating a mixture of 50% water and 50% ethylene-glycol at a rate of 9 L/min. The heat loads were performed using a kapton skin heater attached to each capillary evaporator saddle (70 x 15 mm, 14 Ohms), connected to a DC power supply with deviation of ± 1.0%. All tests were performed without pre-conditioning procedures prior the startups and without temperature control of the CC. The liquid inventory was 25 grams of high grade acetone, keeping the CCs with 50% of void fraction in the cold mode. Details on the LHP geometric characteristics are presented by Table 1 and the power cycles used to test the device are presented by Table 2.

Table 1. Geometric characteristics of the TCD-LHP2.

| | | | |
|---|---|---|---|
| *Capillary Evaporator* | | *Liquid Line* | |
| Total Length (mm) | 100 | Outer Diameter (mm) | 4.85 |
| Active Length (mm) | 67 | Inner Diameter (mm) | 2.85 |
| Outer/Inner Diameter (mm) | 19.0 / 16.5 | Length (mm) | 850 |
| Material | Stainless steel grade 316L (ASTM) | Material | Stainless steel grade 316L (ASTM) |
| *UHMW Polyethylene Wick* | | *Condenser* | |
| Pore Radius ($\mu$m) | 6 | Outer Diameter (mm) | 4.85 |
| Permeability ($m^2$) | $10^{-13}$ | Inner Diameter (mm) | 2.85 |
| Porosity (%) | 50 | Length (mm) | 1000 |
| Diameter (OD/ID) mm | 16.5 / 7.0 | Material | Stainless steel grade 316L (ASTM) |
| Grooves height, width, angle | 2.0 mm/2.5 mm/26° | | |
| Number of Grooves | 15 | | |
| *Compensation Chamber* | | *Vapor Line* | |
| Volume ($cm^3$) | 20 | Outer Diameter (mm) | 4.85 |
| Screen mesh | # 200 Stainless steel grade 304L (ASTM) | Inner Diameter (mm) | 2.85 |
| TCD-LHP2 OD/length (mm) | 19/95 | Length (mm) | 550 |
| Material | Stainless steel grade 316L (ASTM) | Material | Stainless steel grade 304L (ASTM) |

Table 2. Power cycles applied to the TCD- LHP2.

| Profile | Power Cycle (W) | Startup Power (W) |
|---|---|---|
| 1 | 20-2-30-2-40 | 20 |
| 2 | 40-10-60-5-20-80 | 40 |
| 3 | 2-10-2-30-50-2 | 2 |
| 4 | 60-5-80-2-40-10 | 60 |
| 5 | 2-5-1-2-1-5 | 2 |

The proposed mathematical model was used to correlate the data generated by the experimental results of the TCD-LHP2 operating with a condensation temperature of 5 °C. More details on the LHP experimental program and performance evaluation along time are given by Ref. [22].

## EXPERIMENTAL RESULTS AND DISCUSSION

The TCD-LHP2 was tested at horizontal orientation with a controlled room temperature ranging between 18 and 20 °C, without preconditioning procedures or control on the CC temperature. During the experimental tests, the LHP performance and capability on transporting heat was analyzed, which showed acceptable results without indication of capillary evaporator failure. Figure 4 shows the results of two power cycles applied to the LHP,

where Tevap is the average temperature of thermocouples TC-05 to TC-08 and CC is the average temperature of thermocouples TC-02 and TC-03.

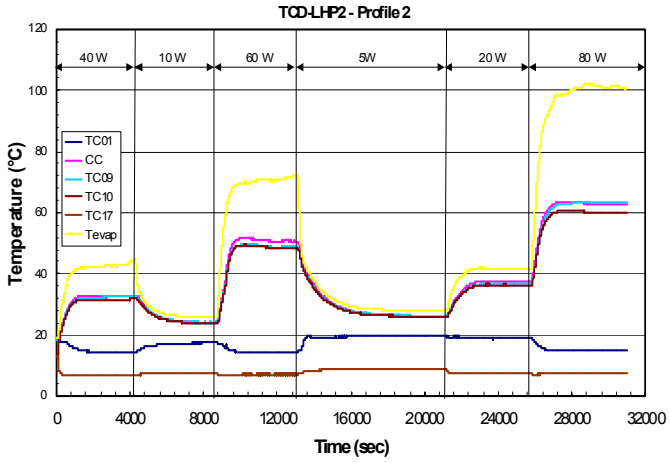


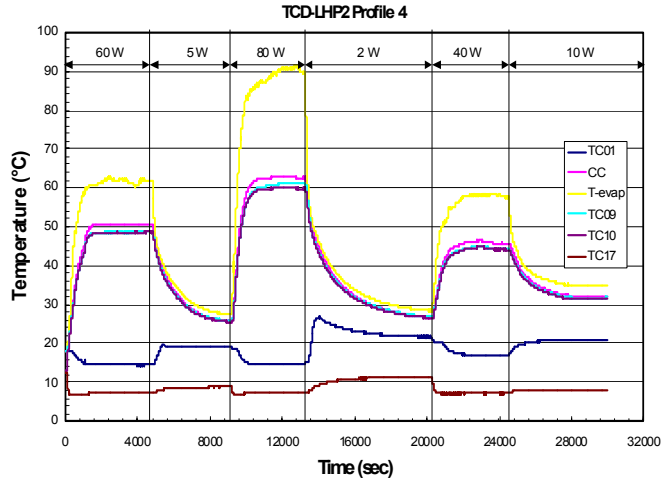


Figure 4. TCD-LHP2 experimental test results.

The continuous operation of the TCD-LHP2 shows the potential in using acetone as an alternative working fluid. Acceptable performance has been observed during the operation when the TCD-LHP2 had to manage the sudden changes in the applied heat load. It can be observed fast transients and reliable operation when the heat loads were changed, reaching the steady state condition in short time. For the entire range of applied heat load (1 to 80 W), the TCD-LHP2 presents acceptable temperature control of the heat source even when an alternative working fluid such as acetone is used, as presented by Fig. 5. The overall test results regarding the thermal resistance between the capillary evaporator and the CC is presented by Fig. 6.

The TCD-LHP2 has accomplished the entire test program with acceptable results, which were all in agreement along time without NCG influence, as the temperatures changes were always within the thermocouples deviation. Even though no influence of NCGs have been verified so far, further investigations on this matter are still required.

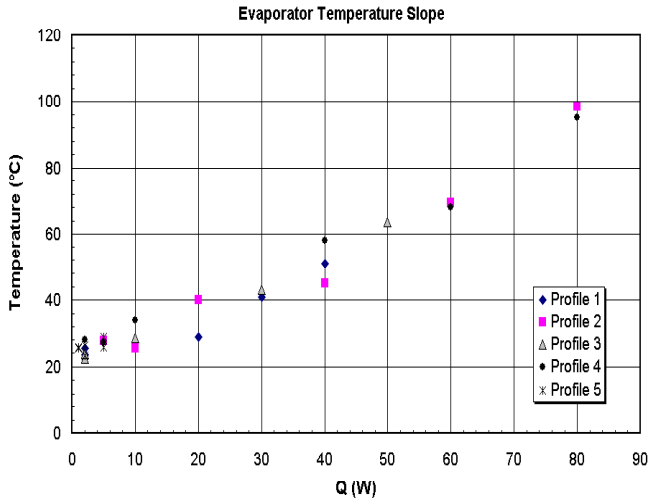


Figure 5. Capillary evaporator temperature slope.

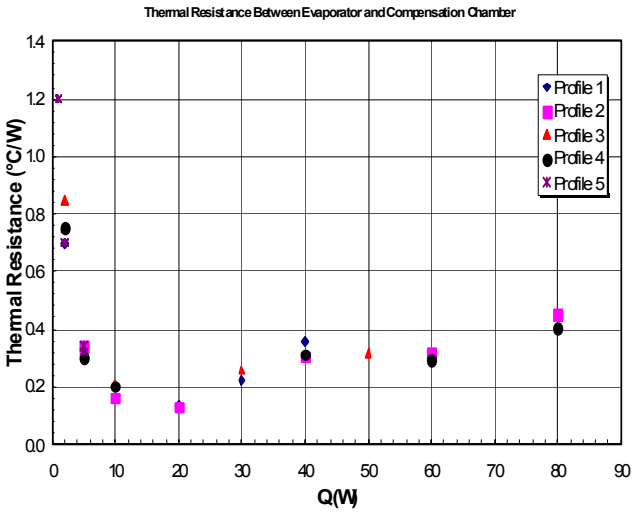


Figure 6. Thermal resistances between evaporator and CC.

The experimental results presented above were used to adjust the mathematical model for proper validation in ground conditions. Furthermore, the model can be used for space conditions where the LHP behavior on a low Earth orbit is necessary to be evaluated.

## MODELING OF LOOP HEAT PIPE AT GROUND TEST CONDITIONS

The tests conditions applied to the experimental tests have been reproduced in the mathematical model, and their parameters were adjusted using the measured temperatures taken throughout the LHP test apparatus. Performing the simulation of the TCD-LHP2 according to the conditions of profile 4, Fig. 7 shows the results

where the mathematical model results are indicated by the continuous lines.

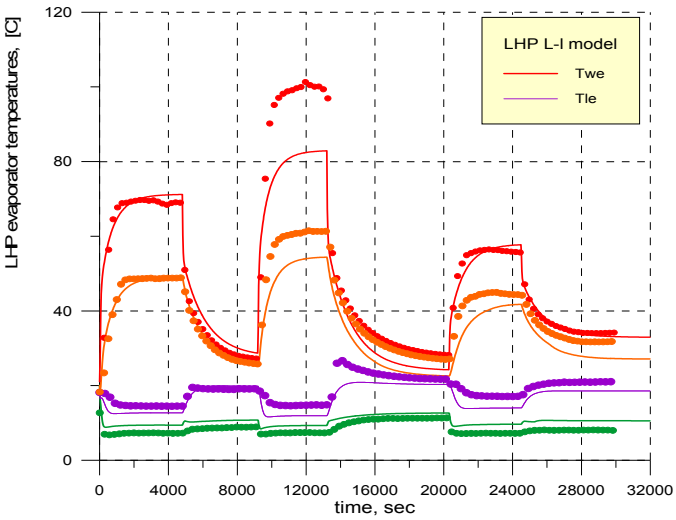


Figure 7. Results of experiment and modeling.

From this graph it is seen that at the maximum heat load (80W), the real thermal conductance from the evaporator wall to the liquid-vapor interface is higher than for 60 W. This can be explained by the fact that either the circular small grooves in the internal surface of evaporator container were partially dried, or the vapor-liquid interface was dislocated slightly towards the primary bulk wick. In either situation, the mathematical model could properly predict the transient behavior of the LHP from the startup until the steady state and also when the heat loads were suddenly changed.

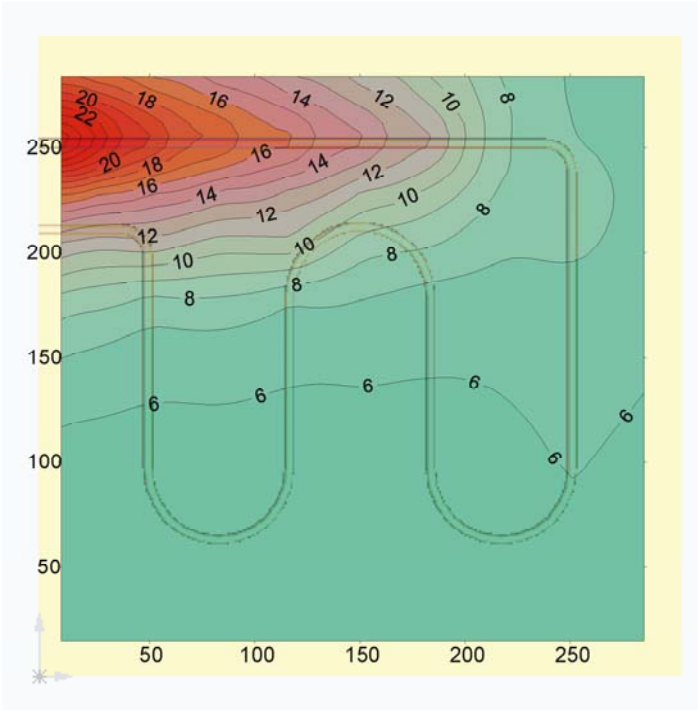


Figure 8. 2-D temperature map of condenser plate (oC) for t=12000 sec (80W)

The temperature distribution along the condensation plate could also be mapped and showed outstanding correlation with the experimental results as presented by Figs. 8 and 9. It can be observed the influence of the vapor at the condenser inlet as the temperatures at the tubing close to outlet are higher than at the opposite side of the plate. The mathematical results show that the LHP condenser is oversized for these particular conditions where a cooling bath was used to promote the heat dissipation, providing therefore a high heat transfer coefficient to an almost constant sink temperature.

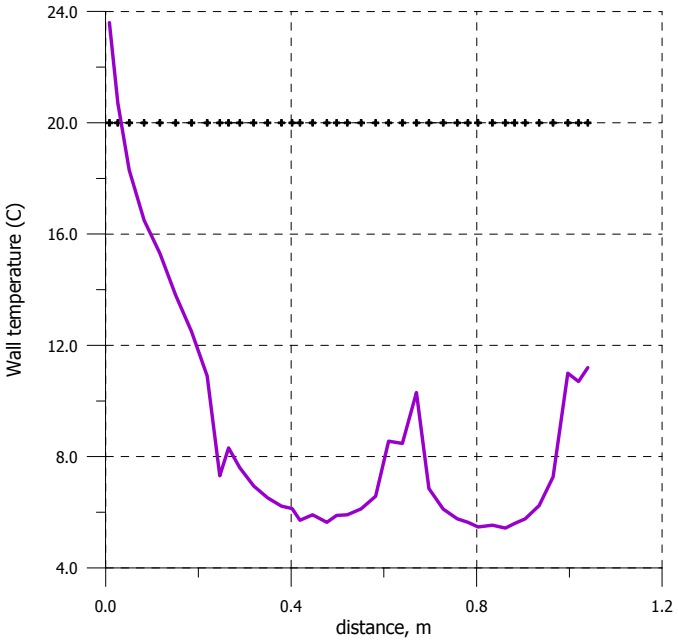


Figure 9. Temperature profile of radiator along condenser tubing at t=12000 sec.

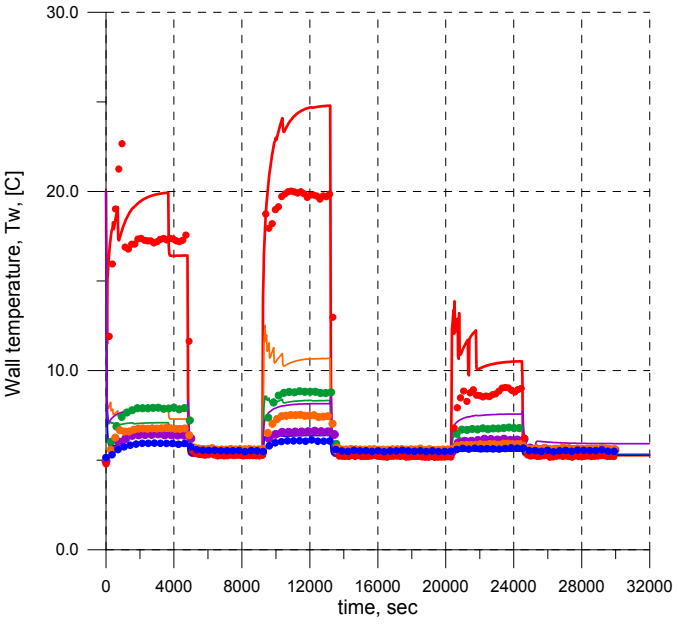


Figure 10. Temperatures on the tubing on the condenser

The calculated and measured temperatures on the condenser are plotted in Fig. 10. The disagreement lies within about 3-4 C except at the maximum load of 80 W. To complete this analysis, Fig. 11 presents the fraction of the condenser actually been used during the process. This figure clearly shows the portion occupied by the fluid in the loop and the active length of the condenser during the LHP operation. From the Figure, it can be noticed that the vapor front is adjusting itself for the new heat load applied to the capillary evaporator, as the flow rate has been changed. In this case, such information is very important to predict the LHP performance under different conditions on the radiator. On the same way, the refinement of this model would greatly contribute to optimize the entire LHP design.

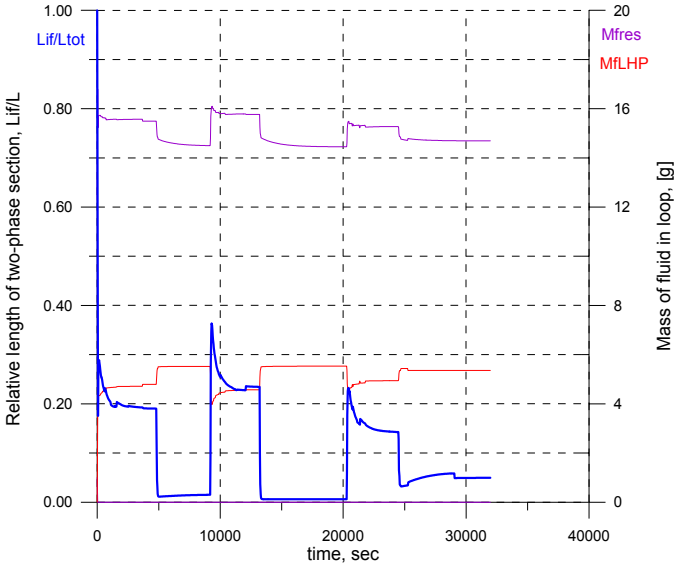


Figure 11. Fraction of opening of condenser (blue line)

As a result of the mathematical model adjusting, the following values of the evaporator parameters were found to fit the experimental results as much as possible:

$G_{ifif}$=1.2; $G_{ifr}$=0.5; $G_{we}$=2.9 $G_{wr}$=0.12 [W/°C], ζ=0.9

In this particular case, such an adjustment is important to validate the current model and then use it to properly model the LHP behavior in space conditions.

## MODELING OF THE LOOP HEAT PIPE BEHAVIOR IN SPACE CONDITION

After adjusting the model to correlate the experimental ground tests, it can then be applied to investigate the LHP behavior in space conditions. The annular flow suggestion for condenser is valid for both 0g and 1g conditions, and fluid viscosity is taken as a function of current temperature, as well as all other fluid properties. However the present model of the evaporator and reservoir does not sensitive to gravity variations. From another hand, the main difference can lay in the phase distribution inside the reservoir: at 0g the liquid will be collected to colder (outer) cap of the reservoir. We expect that this difference could affect temperature profiles of some transient modes, however the temperatures at quasi steady-state patterns are expected to be similar for 1g and 0g.

This analysis is important to verify the expected performance of the LHP in some low orbit. The external fluxes on the radiator have been calculated for the circular orbit of 750 km and inclination of 20° that correspond the orbit of EQUARS satellite being under development at INPE. The side Y+ (velocity vector-oriented at normal mode) has been selected; both nominal (hot) and safe (cold) cases were considered. In this case, the radiator coating used is Teflon-Al film of 125 mkm. The result absorbed heat fluxes are presented by Figure 12. Figure 13 presents the simulation results of the LHP evaporator temperature in the hot case.

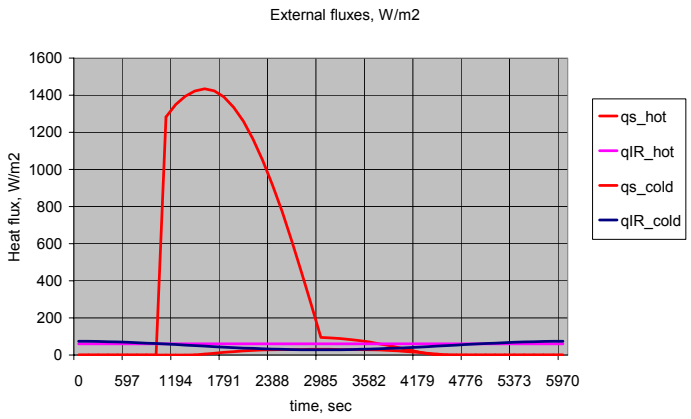


Figure 12. External fluxes on radiator for cold and hot cases.

First, the hot case under heat loads of Q=30 W has been simulated. In was assumed that the CC is perfectly insulated from the ambient by a high efficient MLI. The results shown in Fig. 13 demonstrate that the internal heat transfer from the bayonet to the fluid in the reservoir (1-ζ) is not effective enough to cool down the CC, whereas the parasitic heat input from the evaporator through the wall is very high.

The fraction of opening the condenser is shown by Fig. 14. This value is less than 20% and confirm that there is a possibility to get the temperature down by other means, either by providing a heat transfer from the CC surface to colder ambient or by applying a thermo-electric cooling (TEC) to CC.

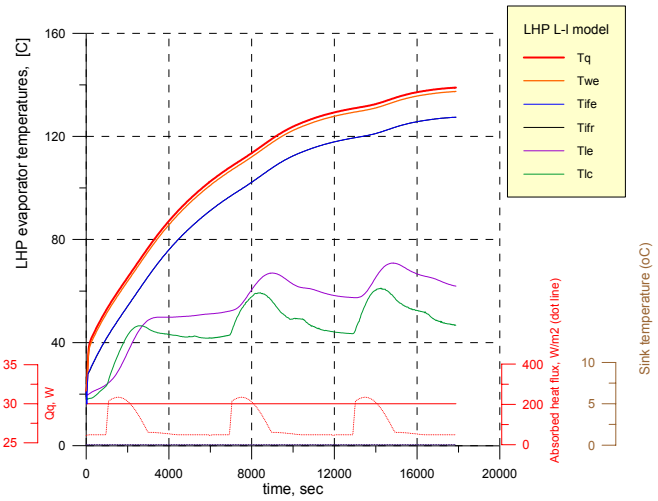


Figure 13. Evaporator temperatures; hot case, Q=30W, reservoir is perfectly insulated.

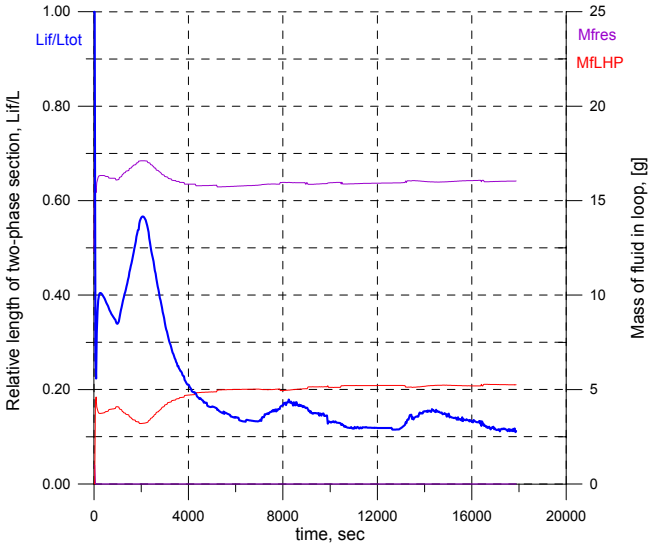


Figure 14. Rate of condenser opening; Space conditions, hot case, Q=30W, reservoir insulated.

The Figure 15 shows the temperatures of the radiator plate picked from various locations along the condenser tubing. It can be observed that the temperature influence of the condenser tubing where the vapor enters it highly influences the temperature at the curves where the liquid (with some degrees of subcooling) is returning to the evaporator by the liquid line. In this particular case, an optimization of the curves positioning in the condenser can be made in order to reduce such an influence.

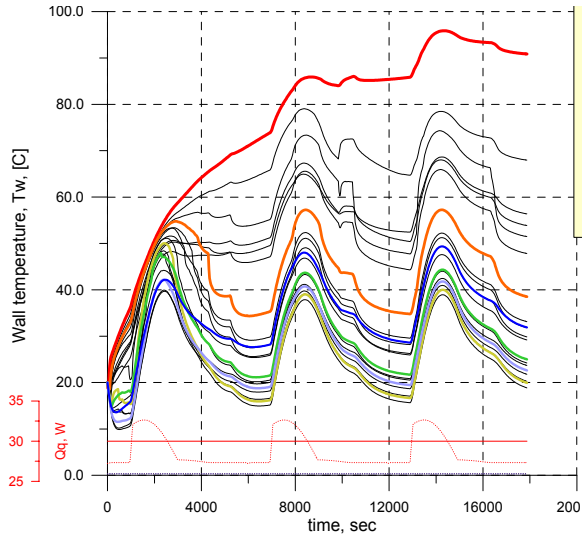


Figure 15. Condenser temperatures; hot case, Q=30W, reservoir insulated.

Figures 16 and 17 show the results of simulation for the case when the reservoir is painted to have a property of ε=0.9 open to a cold ambient having average temperature of 10 °C.

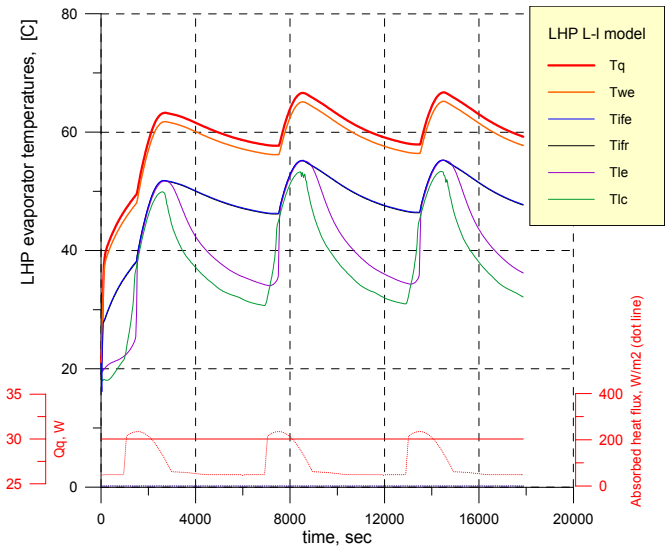


Figure 16. Evaporator temperatures; hot case, Q=30W, reservoir surface is coated to ε=0.9 and exposed to ambient of 10 °C.

One can observe that the fraction of opening increases and temperatures decreases. This is a characteristic of the improved coupling of the CC to a cold ambient, which contributes to improve the LHP performance. From another hand, as it seen from the Fig. 17, at peaks of external heat fluxes, vapor enters the liquid line, which is not desirable.

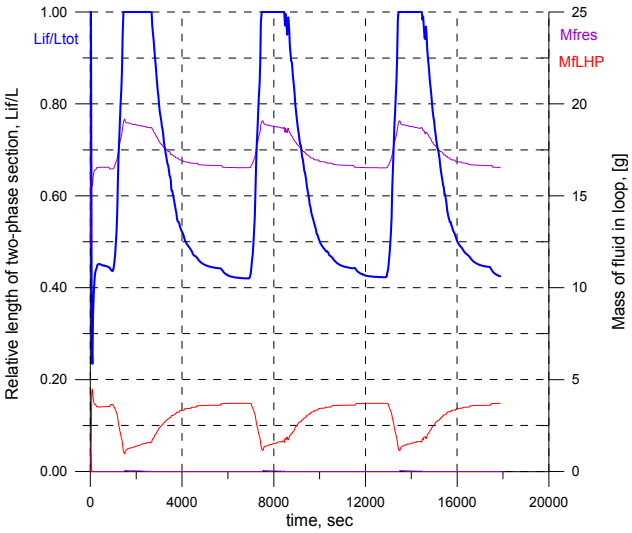


Figure 17 . Rate of opening of condenser for previous case.

Figure 18 presented the 2-D plot of condenser (radiator) temperatures at instants of t=6000 (fraction of opening is ~0.42) and Fig. 19 shows the temperature distribution at t=8000 sec when the condenser is fully open and vapor phase enters the liquid line.

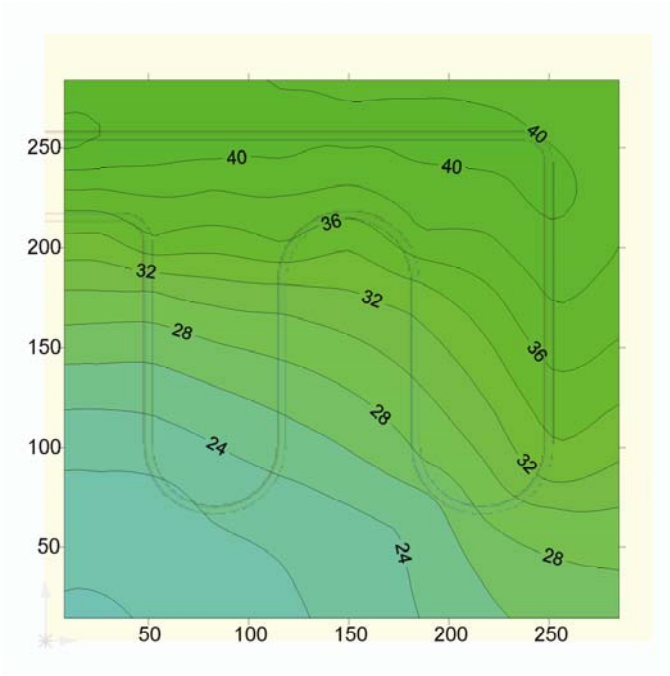

Figure 18 . Condenser 2-D plot – t=6000 sec.

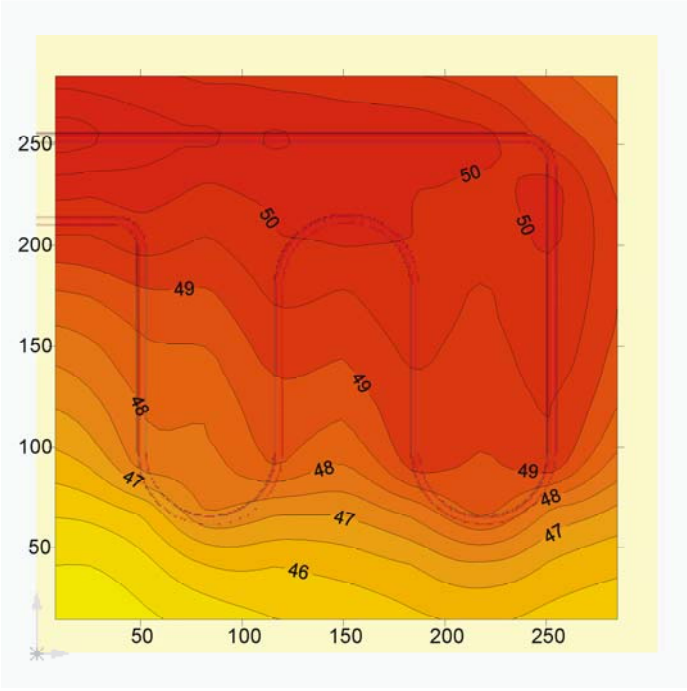

Figure 19 . Condenser 2-D plot – t=8000 sec. – fully open

Figures 20 presents the cold case simulated at the same heat load on the evaporator (30W) and Fig. 21 presents the active length in the condenser (blue line) as well as the mass of fluid in the loop (red) and CC (violet) for the above mentioned heat load.

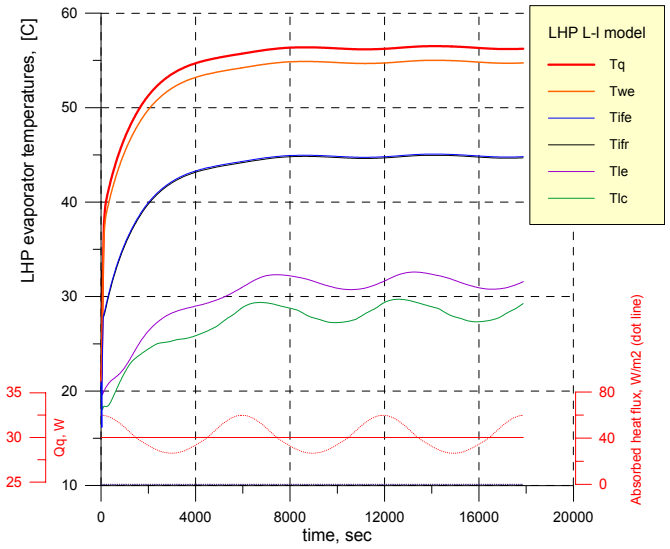


Figure 20. Cold case, evaporator temperatures.

It is also interesting to note that the maximum temperatures at the LHP evaporator saddle (red lines in Figs. 16 and 20) do not present a major change or the hot and cold cases respectively, in spite of the average adsorbed heat fluxes that differ from 42 to 95.5 W/m$^2$.

Simulating the hot case again but substituting the acetone for the ammonia, Figs. 22 and 23 show the results for 30 W applied to the LHP evaporator.

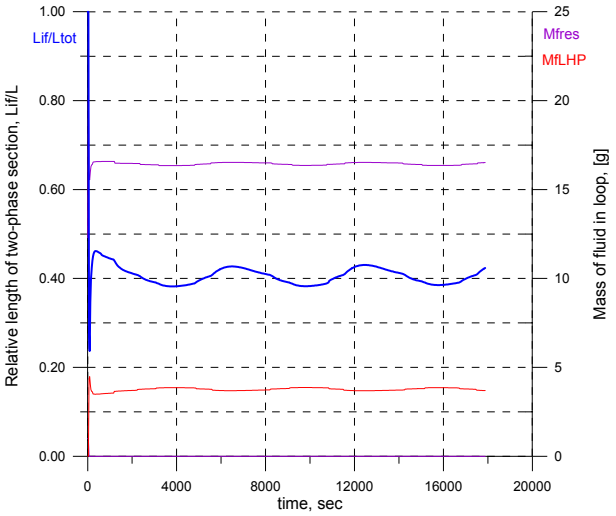


Figure 21. Cold case.

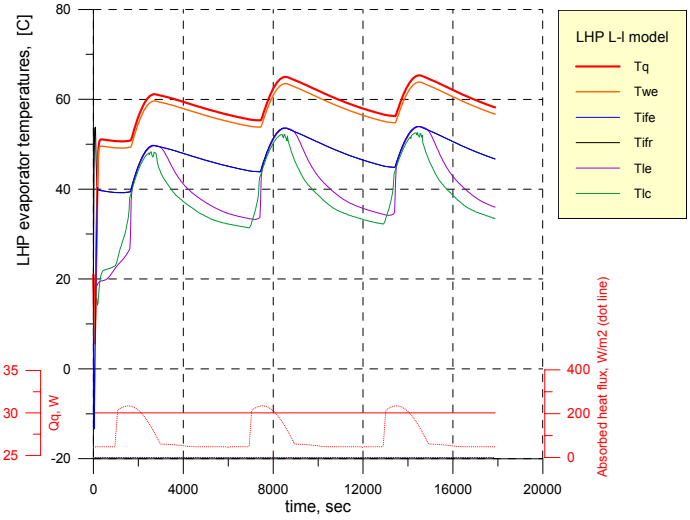


Figure 22. Hot case – ammonia.

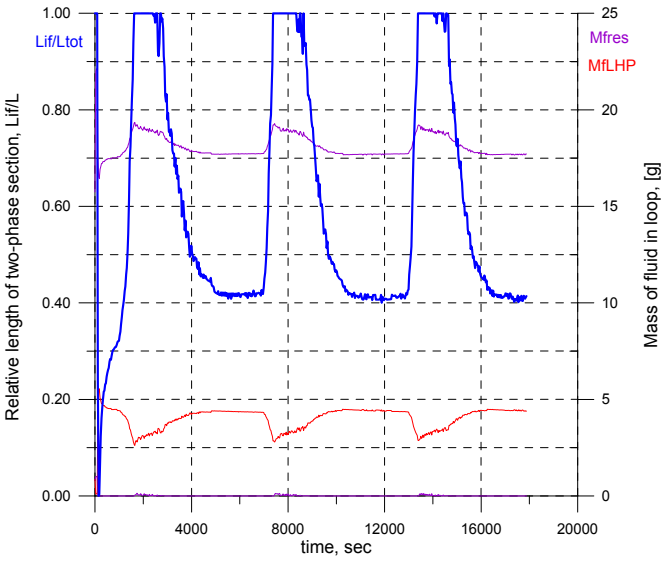


Figure 23. Hot case – ammonia.

It is very interesting to note that almost nothing was changed despite of the so-used ammonia being applied to this simulation: the evaporator temperatures are still high and vapor phase periodically enters the liquid line.

Figure 24 presents the sensibility of the LHP system to the possible control by TEC was investigated. The fluid was changed back, from ammonia to acetone.

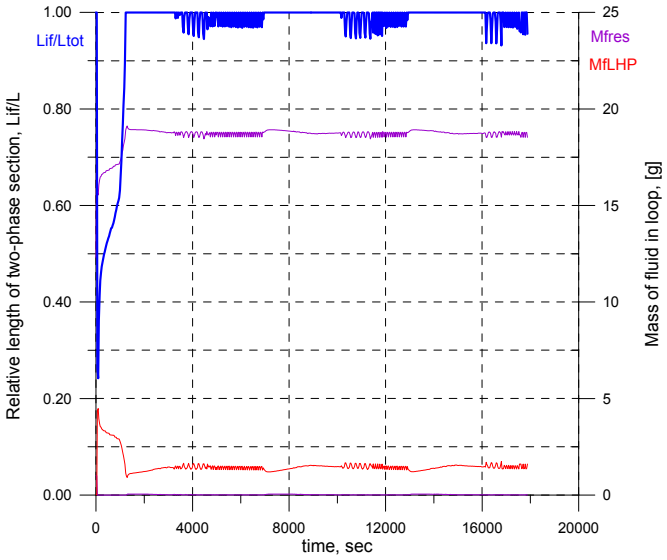


Figure 24. Acetone, TEC on reservoir (-1W).

It is very notable, that so minor cooling power ($Q_r$= 1 W) switches the LHP to a certainly not-operational mode, when the condenser is almost constantly fully open.

Figures 25 shows the heat load that was adjusted to limit the fraction of condenser opening to about 80% and maximal temperature at the evaporator saddle to about 50 °C. For the same conditions, Fig. 26 shows the results for the active length in the condenser and the amount of fluid in the loop.

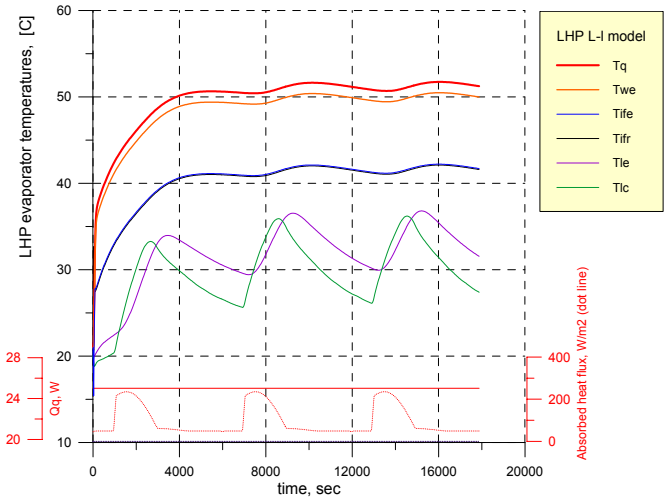


Figure 25. Acetone, Q=25 W - hot case.

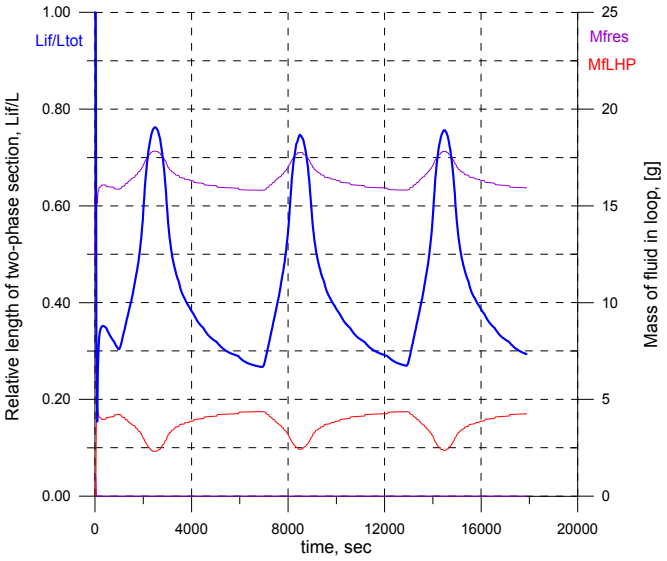


Figure 26. Hot case 25 W.

These requirements are valid for a heat load of 25 W. This heat load was announced as a limit for this LHP with given radiator size and given Space application (i.e. radiator placing on satellite and external conditions). The only limiting factor is the size of radiator. If radiator dimensions were increased, the maximal heat load could be increased up to 80W, as tested for ground conditions. The reason lies in the fact that the present LHP operates far from its capillary limit as demonstrated by the experimental results and modeling.

## DISCUSSION OF RESULTS AND CONCLUSION

The combined model, consisted of a detailed model of condenser and coarse model of evaporator/CC, is able to predict the LHP transient behavior within 3-4 °C of accuracy (for a heat load range between 2 and 60 W) if the uncertain parameters are adjusted by experimental results. The experimental results used to validate this model were gathered for a LHP operating at a maximum heat load of 80 W using acetone as working fluid. Whereas at maximal heat loads, when density of heat flux is high enough to make partial dry-out of circular grooves or to dislocate the liquid-vapor interface (Q=80W for given design), the difference may reach 18 °C on the evaporator saddle.

Given the simplified design of the cylindrical evaporator/CC assembly it is a very feasible LHP for applications in conditions when additional TEC control is applied to the CC. For this kind of control, if required, a heat load less than 1 W is more than enough.

Maximal power for this LHP design is 80W (for an enhanced radiator for Space conditions). The choice of acetone as working fluid presents acceptable operation as the LHP operates far from its capillary limit.

## ACKNOWLEDGMENTS

This work has been supported by the National Institute for Space Research (INPE) and by Fundação de Amparo a Pesquisa no Estado de São Paulo (FAPESP/Brazil), grants 03/08365-6 and 03/11477-0.

## REFERENCES

1. Stenger, F.J. "Experimental feasibility study of water-filled capillary-pumped heat- transfer loops", Washington, D.C., NASA, 1966, NASA TM X-1310.
2. Gerasimov, Y. F., Maidanik, Y. F., Dolgirev, Y. Y., "Some results of investigation of low-temperature heat pipes operating against gravity field (in Russian)", Eng.Phys.J, Vol 30 N4, 1976, pp.581-586
3. Maidanik, Y. F., Vershinin S, Kholodov V, Dolgirev J., "Heat Transfer Apparatus", US Patent, May 7, 1985, No. 4515209.
4. Maidanik, Y. F., Fershtater YG., "Theoretical basis and classification of loop heat pipes and capillary pumped loops", Proceeding of the 10th International Heat Pipe Conference. September 21-25, 1997, Stuttgart (Germany), pp. 1-15.
5. Nikitkin, M., Cullimore, B., "CPL and LHP technologies: what are the differences, what are the similarities", SAE Paper 981587. Proceeding of the 28th ICES. July 13-16, 1998, Danvers (Massachusetts, USA), pp. 1-10.
6. Butler, D., Hoang, T., "The enhanced capillary pumped loop flight experiment: a prototype of the EOS platform thermal control system". Proceedings of the 26th AIAA Thermophysics Conference, Honolulu, 1991, AIAA 91-1377.
7. Ku, J., Ottenstein, L., Butler, D., "Performance of CAPL 2 flight experiment", Proceedings of the 26th International Conference on Environmental Systems, Monterey, CA, 1996, SAE Paper Series 961432.
8. O'Connell, T., Hoang, T., Ku, J., "Investigation of power turn down transients in CAPL-1 flight experiment", Proceedings of the 30th AIAA Thermophysics Conference, San Diego, CA, 1995, paper AIAA 95-2067.
9. Kiper, A. M., Swanson, T. D., McIntosh, R., "Exploratory study of temperature oscillations related to transient operation of a capillary pumped loop heat pipe", Proceedings, ASME Nat. Heat Transfer Conf., Houston, 1988, p.353-359.
10. Kolos, K. R., Herold, K. E., "Low frequency temperature and fluid oscillations in Capillary Pumped Loops", Proceedings of National Heat Transfer Conference, Baltimore, MD, 1997, paper AIAA 97-3872.
11. Maidanik, Y., Fershtater, Y., Pastukhov, V. G., Chernysheva, M., "Experimental and theoretical investigation of startup regimes of two-phase capillary pumped loops", Proceedings of the 23rd International Conference on Environmental

Systems, Colorado Springs, CO, 1993, SAE Technical Paper Series 932305.
12. Butler, D., Ottenstein, L., Ku, J., "Flight testing of Capillary Pump Loop flight experiment", Proceedings of the 25th International Conference on Environmental Systems, San Diego, CA, 1995, SAE Technical Paper Series 951566.
13. Butler, D., Ottenstein, L., Ku, J., "Design evolution of the Capillary Pumped Loop (CAPL 2) flight experiment". Proceedings of the 26th International Conference on Environmental Systems, Monterey, CA, 1996, SAE Paper 961431.
14. Antoniuk, D., Nienberg, J., "Analysis of Salient Events from the Two-phase Flow (TPF) Thermal Control Flight Experiment". Proceedings of the 28th International Conference on Environmental Systems. Danvers, Massachusetts, July 13-16, 1998, SAE Paper 981817, p.1-13.
15. Cao, Y., Faghri, A., "Analytical solution of flow and heat transfer in a porous structure with partial heating and evaporation on the upper surface", International Journal of Heat and Mass Treansfer, Vol. 17, N. 10, 1994, pp. 1525-1533.
16. Khrustalev, D., Faghri, A., "Heat transfer in the inverted meniscus type evaporator at high heat fluxes", International Journal of Heat and Mass Treansfer, Vol. 38, N 16, 1995, pp. 3091-3101.
17. Fugus, C., Bray, Y. Le, Bories, S., Prat, M., "Heat and mass transfer with phase-change in a porous structure partially heated: continuum model and pore network simulation", Int. Journal of Heat and Mass Transfer, V 42, 1999, pp. 2557-2569.
18. Begg, E., Khrustalev, D., Faghri, A., "Complete Condensation of Forced Convection Two-Phase Flow in a Miniature Tube". Journal of Heat Transfer, Vol. 121, 1999, pp. 904-915.
19. Muraoka, I., Vlassov, V. V., "Numerical Model of the CPL for Microgravity Experiment", Proceeding of the 6th International Heat Pipe Symposium – 2000 (6IHPS-2000), 5-9 November 2000, Chiang Mai, Thailand, ISBN 974-657-448-5, pg 94-103.
20. Cullimore, B., Baumann, J., "Steady-State and Transient Loop Heat Pipe Modeling", Proceedings of the 30th ICES, July 10-13, 2000, Toulouse, France. Paper 2000-01-2316, pp. 1-9.
21. Vlassov, V.V., Schlitt, R., Bondendieck, F. Two-Level Modeling of Capillary Pumped Two-Phase Loops. Proceeding of Two-Phase 2003 International Two-Phase Thermal Control Technology Workshop 2003, ESA/ESTEC, Noordwijk, The Netherlands, September 15 to 17, 2003
22. Riehl, R. R., Siqueira, T. C. P. A., "Evaluating Loop Heat Pipes Performances Regarding Their Geometric Characteristics, 35th International Conference of Environmental Systems, Rome, Italy, July 11-14, 2005, paper # 2005-01-2882.
23. Vargaftic, N.B., Vinogradov Yu.K., Yargin V.S. Handbook of Physical properties of Liquids and Gases. Begell House, Inc., NY, 1996.

## CONTACT

Valeri V. Vlassov, Dr.
National Institute for Space Research
Space Mechanics and Control Division
INPE-DMC/Satelite
Av. Dos Astronautas 1758, 12227-010
Sao Jose dos Campos, SP – Brazil
Phone: 55 12 3945-6206 / Fax: 55 12 3945-6226
E-Mail: vlassov@dem.inpe.br

## DEFINITIONS, ACRONYMS, ABBREVIATIONS

| *Symbol* | *Description* |
|---|---|
| A | area |
| C | specific heat |
| G | thermal conductance (W/K) |
| h | heat transfer coefficient |
| k | thermal conductivity |
| L | length |
| M | mass |
| $\dot{m}$ | mass flow rate |
| P | pressure |
| Q | heat flux |
| q | heat flux density (W/m2) |
| r | radius |
| R | internal radius of tube |
| s | coordinate, either x or y |
| T | temperature |
| V | volume |
| u | velocity along x-axis |
| $\Delta$y | elevation |
| x | coordinate or mass fraction of vapor |
| | *Greeks* |
| $\delta$ | thickness |
| $\varepsilon$ | emissivity |
| $\lambda$ | latent heat of evaporation |
| $\mu$ | dynamic viscosity |
| $\rho$ | density |
| $\sigma$ | surface tension |
| $\sigma$ | Stefan-Boltzman constant |
| $\xi$ | friction factor |
| $\tau$ | tangential stress |
| | |
| | *Superscripts* |
| " | vapor phase |
| ' | liquid phase |
| | *Subscripts* |
| e | evaporator |
| f | fluid |
| h | hydraulic or convective |
| l | liquid |
| sat | saturation |
| q | saddle (at interface to equipment) |
| r, res | reservoir |
| w | wall |
| $\delta$ | at interface |